

ARTICLE

Physical properties of Si₂Ge and SiGe₂ in Hexagonal Symmetry: First-Principles Calculations

Ying-bo Zhao^a, Shi-xuan Lin^a, Qing-yang Fan^{b*}, Qi-dong Zhang^{c*}

a. School of Mechanical and Electrical Engineering, Xi'an University of Architecture and Technology, Xi'an 710055, China

b. School of Information and Control Engineering, Xi'an University of Architecture and Technology, Xi'an 710055, China

c. School of Microelectronics, Xidian University, Xi'an, 710071, China

(Dated: Received on August 13, 2020; Accepted on October 8, 2020)

We predict two novel group 14 element alloys Si₂Ge and SiGe₂ in *P6₂22* phase in this work through first-principles calculations. The structures, stability, elastic anisotropy, electronic and thermodynamic properties of these two proposed alloys are investigated systematically. The proposed *P6₂22*-Si₂Ge and *P6₂22*-SiGe₂ have a hexagonal symmetry structure, and the phonon dispersion spectra and elastic constants indicate that these two alloys are dynamically and mechanically stable at ambient pressure. The elastic anisotropy properties of *P6₂22*-Si₂Ge and *P6₂22*-SiGe₂ are examined elaborately by illustrating the surface constructions of Young's modulus, the contour surfaces of shear modulus, and the directional dependence of Poisson's ratio; the differences with their corresponding group 14 element allotropes *P6₂22*-Si₃ and *P6₂22*-Ge₃ are also discussed and compared. Moreover, the Debye temperature and sound velocities are analyzed to study the thermodynamic properties of the proposed *P6₂22*-Si₂Ge and *P6₂22*-SiGe₂.

Key words: Group 14 element alloys, Stabilities, Elastic anisotropy properties, Electronic properties

I. INTRODUCTION

Discovering new group 14 element allotropes and group 14 element alloys has continuously inspired the worldwide effort in academia and industry, as their novel properties and improved performance exhibited over the past several decades never fail to fascinate researchers. Recently, scientific research is ongoing into the steps of the fundamental understanding and technological improvements of group 14 alloys, through theoretical predictions and experiments, especially for the Si-Ge alloys due to their merits and possible applications [1–8].

It is well known that silicon is the most basic and second most abundant semiconductor material on earth, which is commonly used and considered as the cornerstone of the modern semiconductor industry. However, Si in diamond phase is an indirect band-gap semiconductor material, and direct band-gap Si allotropes are still scarce [9–14], which limits their application in photoelectric industry [15–17]. Therefore, more and more researchers have begun exploring new group 14 element allotropes, and studying physical properties of

group 14 element alloys [18–31]. For group 14 element Si-Ge alloys, Si₈Ge₄ and Si₄Ge₈ in *P4₂/mnm* phase [18], Si_{0.5}Ge_{0.5} in *Cmmm* phase [19], and Si_{0.7}Ge_{0.25} and Si_{0.5}Ge_{0.5} in Lonsdaleite phase [20] are all indirect band-gap alloys. However, Si-Ge alloys can transform from indirect bandgaps into direct bandgaps to some extent, and a great deal of work has focused on it. For example, when adjusting the stoichiometric ratio of silicon to germanium to 1:3, the Si-Ge alloy (Si_{0.25}Ge_{0.75}) became a direct band-gap semiconductor in Lonsdaleite phase [20]. Also, when the stoichiometric ratios of silicon to germanium are 1:2 in *P6₃/mmc* and 2:1 in *Cmcm* phase, all the materials reported in Ref.[21] were direct band-gap semiconductors.

Moreover, incorporating germanium into Si allotropes has attracted extensive interests due to the fact that silicon-based semiconductors doped with germanium have shown a high electronic property while retaining the thermal and mechanical stability of silicon [21–27]. Fan *et al.* [21] investigated the physical properties of Si, Ge and Si-Ge alloys in *oC12* and *hP12* phases, among which Si₁₂, Ge₁₂ and Si₈Ge₄ alloys had direct band-gaps and show strong absorption ability. Moriguchi *et al.* [22] predicted Si-Ge alloys in an ideal *Fd-3m* phase, and these alloys were reported as direct wide-gap semiconductors. Schäffler *et al.* [23] developed a high-mobility Si-Ge heterojunction. Fan

* Authors to whom correspondence should be addressed. E-mail: anqy@xauat.edu.cn, qdzhang@xidian.edu.cn

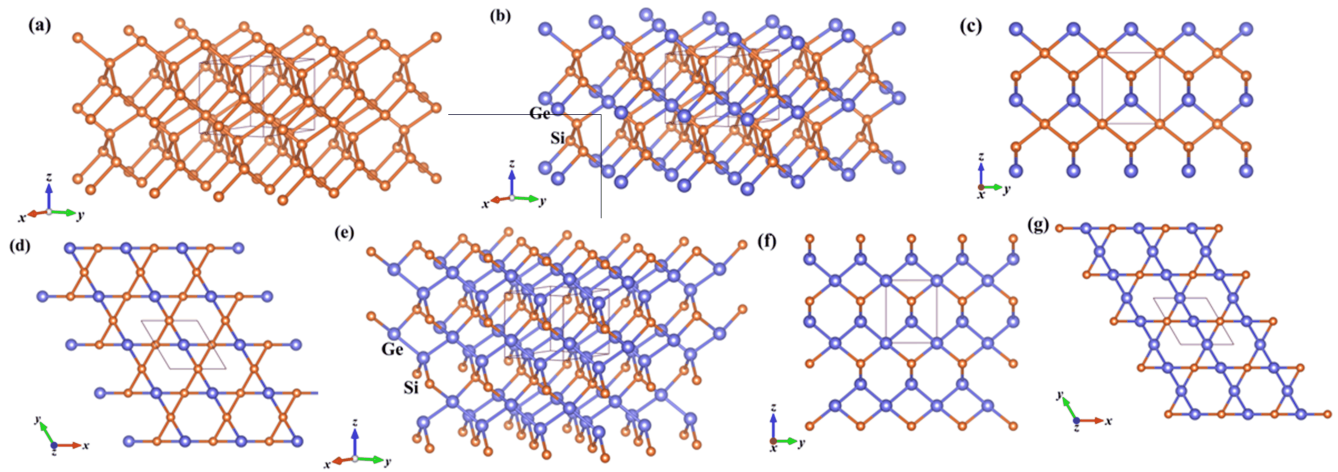


FIG. 1 The crystal structures of (a) Si or Ge allotrope in $P6_222$ phase, (b) Si_2Ge alloy in $P6_222$ phase and its structure viewed along (c) the x -axis and (d) the z -axis, (e) SiGe_2 alloy in $P6_222$ phase and its structure viewed along (f) the x -axis and (g) the z -axis.

et al. [24] predicted a new metastable silicon allotrope $t\text{-Si}_{64}$, which was in $I4_1/amd$ phase. Owing to the minimum thermal conductivity of $t\text{-Si}_{64}$ found to be greatly smaller than that of diamond-Si, it was reported that the Si-Ge alloys in $I4_1/amd$ phase can be used as potential thermoelectric materials. Song *et al.* [25] proposed Si_{16} , Ge_{16} and Si-Ge alloys in $C2/m$ phase, and the results indicate that the absorption ability of these alloys is better than that of diamond-Si.

In this work, two group 14 element alloys Si_2Ge and SiGe_2 in $P6_222$ phase are proposed. The crystal structures of $\text{Si}_{3-x}\text{Ge}_x$ ($x=0, 1, 2, 3$), including two proposed alloys (Si_2Ge and SiGe_2) and their allotropes (Si_3 and Ge_3) in $P6_222$ phase are discussed. The mechanical and dynamic stabilities of the newly predicted alloys are verified by analyzing elastic constants and phonon dispersion spectra, respectively. Furthermore, the elastic anisotropy properties of $\text{Si}_{3-x}\text{Ge}_x$ ($x=0, 1, 2, 3$) in $P6_222$ phase are investigated in detail.

II. THEORETICAL METHODS

Herein, we carried out the project by using the density functional theory (DFT) [32, 33] based on the Cambridge Serial Total Energy Package (CASTEP) plane-wave code [34]. The theoretical calculations were performed with the Perdew-Burke-Ernzerhof (PBE) functional of the generalized gradient approximation (GGA) [35]. The interactions between the ionic core and valence electrons were represented with the ultrasoft pseudopotentials. In addition, the elastic moduli such as the bulk modulus, shear modulus and Young's modulus were estimated by the Voigt-Reuss-Hill approximation. The Broyden-Fletcher-Goldfarb-Shanno (BFGS) [36] minimization scheme was utilized for geometry optimization of Si_2Ge and SiGe_2 in $P6_222$ phase. The

phonon frequency was obtained by the linear response theory [37]. Moreover, the Heyd-Scuseria-Ernzerhof (HSE06) hybrid functional [38] was adopted for calculating the electronic band structures of Si_2Ge and SiGe_2 in $P6_222$ phase. The high k -point separation with a grid spacing (less than 0.025 \AA^{-1}) across the Brillouin zone ($12 \times 12 \times 10$ for Si_2Ge and $12 \times 11 \times 9$ for SiGe_2) was achieved using the Monkhorst-Pack scheme [39]. Lastly, both the plane wave cut-off energies used for property prediction and structural optimization of Si_2Ge and SiGe_2 in $P6_222$ phase were 340 eV, ensuring good convergence of energies and computed structures in this work.

III. RESULTS AND DISCUSSION

The crystal structures of the proposed Si_2Ge and SiGe_2 alloys are comprised of the lattice similar to those of their allotropes (Si_3 and Ge_3) in $P6_222$ phase [40] as shown in FIG. 1 (a). The crystal structures of the proposed Si_2Ge and SiGe_2 in $P6_222$ phase are shown in FIG. 1(b)–(g), and the orange and cyan spheres represent the silicon and germanium atoms, respectively. The Si_2Ge and SiGe_2 also belong to the hexagonal symmetry group and their crystal structures contain several zigzag six-membered atom rings. There are three atoms in a conventional cell, with the crystallographic sites of Si_2Ge occupied at Si1 (0.50000, 0.00000, -0.00592), Si2 (0.00000, 0.50000, 0.67270) and Ge1 (0.50000, 0.50000, 0.33322), and SiGe_2 occupied at Si1 (0.00000, 0.50000, 0.66692), Ge1 (0.50000, 0.00000, -0.00599) and Ge2 (0.50000, 0.50000, 0.33906). When viewed along the x - and z - axes, the crystal structures of Si_2Ge and SiGe_2 in $P6_222$ are shown in FIG. 1 (c) and (d), (f) and (g), respectively.

At ambient pressure, the crystal density ρ and the

TABLE I The crystal density (ρ in g/cm³), the volume of the conventional cell (V in Å³), and the lattice parameters (a , b , and c in Å) of Si_{3-x}Ge_x ($x=0, 1, 2, 3$) in $P6_222$ phase calculated with the PBE method.

Space group	Materials	ρ	V	a	b	c	$\beta/(^\circ)$
$P6_222$	Si ₃	2.574	54.355	3.9041		4.1178	120.00
	Si ₂ Ge	3.742	57.139	3.9786	3.9791	4.2027	120.82
	SiGe ₂	4.760	60.443	4.0154	4.0694	4.2910	120.43
	Ge ₃	5.647	64.039	4.1102	4.3771	120.00	
$Fd-3m$	Si	2.285	40.061	5.4653			
				5.430 [41]			
	Ge	5.223	46.154	5.6941			
				5.660 [41]			

volume of the conventional cell V of Si_{3-x}Ge_x ($x=0, 1, 2, 3$) in $P6_222$ phase, including two allotropes (Si₃ and Ge₃) and their alloys (Si₂Ge and SiGe₂), together with Si and Ge in diamond phase ($Fd-3m$, No.227) are listed in Table I. It can be seen that the density ρ of Si_{3-x}Ge_x ($x=0, 1, 2, 3$) gets higher gradually from 2.574 g/cm³ to 5.647 g/cm³ with increasing the incorporation of germanium atoms, which is due to that the relative atomic mass of silicon obviously weighs less than that of germanium, as well as owing to that the increase rate of the Si_{3-x}Ge_x ($x=0, 1, 2, 3$) volume V is slower than that of the molecular mass. At ambient pressure, the lattice parameters of Si₂Ge and SiGe₂ in $P6_222$ phase, together with Si and Ge in diamond phase are also listed in Table I. As can be seen, the lattice parameters of diamond-Si ($a=5.465$ Å) and diamond-Ge ($a=5.694$ Å) are calculated using the PBE method, and the data are in excellent agreement with the reported experimental data (Si: $a=5.430$ Å [41] and Ge: $a=5.660$ Å [41]). Herein, the lattice parameters of diamond-Si and diamond-Ge are also calculated using the LDA method, with a values of 5.375 Å and 5.545 Å, respectively. Clearly, the PBE method is more authentic, and thus Si-Ge alloys will also be calculated by this method for the following discussions. The lattice parameters of Si₂Ge in the conventional cell are $a=b=3.979$ Å, $c=4.203$ Å and $\beta=120.82^\circ$; and for SiGe₂ the lattice parameters are $a=4.015$ Å, $b=4.069$ Å, $c=4.291$ Å and $\beta=120.43^\circ$ at ambient pressure. It is obviously seen that the higher the germanium/silicon ratio increases, the larger the lattice parameters will be obtained. For instance, the a and c values of SiGe₂ are 0.9% and 2.1% larger than those of Si₂Ge, respectively, and this is due to that the atomic radius of Si is smaller than that of Ge. It should also be noted that the bulk modulus (B in GPa) is strongly related to the interatomic distance in dense covalent systems, as the average distance between adjacent atoms is inversely proportional to B [42]. For instance, the B (85 GPa) of Si₂Ge is larger than that of SiGe₂ (B : 73 GPa), and the bond length of Si₂Ge between two silicon atoms is 2.384 Å and the bond length between silicon and germanium atoms is 2.448 Å. For SiGe₂, the bond length

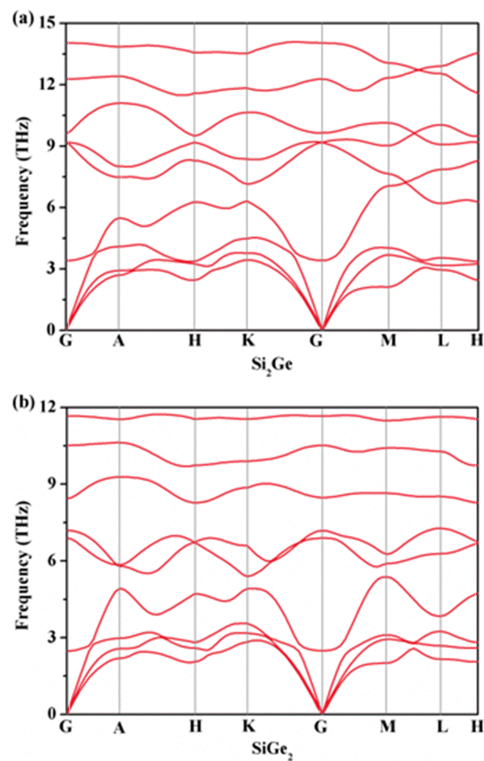


FIG. 2 The phonon spectra of Si₂Ge and SiGe₂ in $P6_222$ phase at ambient pressure.

between two germanium atoms is 2.516 Å, and the bond length between germanium and silicon atoms is 2.451 Å. Clearly, these bond lengths existing in $P6_222$ -Si₂Ge alloy are all shorter than those in $P6_222$ -SiGe₂ alloy.

Since the stability is a key factor which decides the physical performance of materials under certain conditions, the phonon dispersion spectra and elastic constants are analyzed to verify the dynamic and mechanical stability of the proposed alloys. The phonon dispersion spectra of Si₂Ge and SiGe₂ are illustrated in FIG. 2. As can be seen there are no imaginary frequencies at any wave vectors, indicating Si-Ge alloys in $P6_222$ phase are dynamically stable.

The elastic constants of $P6_222$ -Si₂Ge and $P6_222$ -

TABLE II The elastic constants (C_{11} , C_{22} , C_{33} , C_{44} , C_{55} , C_{66} , C_{12} , C_{13} , C_{16} in GPa) and elastic moduli (B , G and E in GPa) of $\text{Si}_{3-x}\text{Ge}_x$ ($x=0, 1, 2, 3$) in $P6_222$ phase.

Materials	C_{11}	C_{22}	C_{33}	C_{44}	C_{55}	C_{66}	C_{12}	C_{13}	C_{16}	B	G	B/G	E	ν
$P6_222\text{-Si}_3$	185		156	78		70	45	58		94	68	1.38	164	0.21
$P6_222\text{-Si}_2\text{Ge}$	172	165	143	69	68	65	36	53	3	85	62	1.37	150	0.21
$P6_222\text{-SiGe}_2$	153	139	127	65	62	56	28	46	2	73	56	1.30	134	0.19
$P6_222\text{-Ge}_3$	123		113	55		47	28	40		64	48	1.33	115	0.20
Diamond-Si	165			87			65			98	70	1.40	170	0.21
	166 [43]			80			64			102				
Diamond-Ge	121			62			49			73	50	1.46	122	0.22
	129 [44]			67			48			77				

SiGe_2 together with those of diamond-Si and diamond-Ge for comparison are all listed in Table II. It is seen that the calculated elastic constants of diamond-Si and diamond-Ge in this work are clearly in good agreement with experimental values [43, 44], indicating the accuracy of our work. The structure of the proposed alloys in this work has nine independent elastic constants (C_{11} , C_{22} , C_{33} , C_{44} , C_{55} , C_{66} , C_{12} , C_{13} and C_{16}), and these elastic constants should satisfy the following generalized Born's mechanical stability criteria for hexagonal symmetry as shown [45]: $C_{11} > 0$, $C_{44} > 0$, $C_{11} > |C_{12}|$, $(C_{11} + C_{22})C_{33} - 2C_{13}^2 > 0$, $C_{66} > 0$. Obviously, all the relevant elastic constants obey the mechanical stability criteria, proving the proposed alloys are mechanically stable. It is known that the C_{11} , C_{22} and C_{33} demonstrate the resistance to linear compression along x -, y - and z - axes, respectively, and the relationship of $C_{11} > C_{22} > C_{33}$ exhibited in Table II shows the z -axis has the weakest linear compression resistance for both $P6_222\text{-Si}_2\text{Ge}$ and $P6_222\text{-SiGe}_2$ alloys. Additionally, the C_{11} , C_{22} and C_{33} of $P6_222\text{-Si}_2\text{Ge}$ are correspondingly larger than those of $P6_222\text{-SiGe}_2$, revealing the resistance to linear compression of $P6_222\text{-Si}_2\text{Ge}$ is higher than that of $P6_222\text{-SiGe}_2$.

The elastic moduli are also shown in Table II, which include the bulk modulus (B), shear modulus (G), Young's modulus (E) and Poisson's ratio (ν). In almost all situations, these four parameters of $\text{Si}_{3-x}\text{Ge}_x$ ($x=0, 1, 2, 3$) show a trend of decrease with increasing the number of germanium atoms. The B and G are obtained by the Voigt-Reuss-Hill approximation. The B and G values of $P6_222\text{-Si}_2\text{Ge}$ are smaller than those of diamond-Si, while the B and G values of diamond-Ge are not larger than those of $P6_222\text{-SiGe}_2$. Moreover, the ratio of B/G is usually utilized to distinguish between the ductility ($B/G > 1.75$) and brittleness ($B/G < 1.75$) for materials [46]. The B/G values of the two proposed $P6_222$ Si-Ge alloys are 1.37 and 1.30, and the B/G values of diamond-Si and diamond-Ge are 1.40 and 1.46, respectively, suggesting all of them exhibit brittle property, and among which $P6_222\text{-SiGe}_2$ displays the most brittle feature. The values of E and ν are achieved by $E = 9BG / (3B + G)$, $\nu = (3B - 2G) / (6B + 2G)$

[47], respectively. Compared with E values, it is found that diamond-Si has the largest E (170 GPa) while diamond-Ge the smallest one (122 GPa), and the E values of $P6_222\text{-Si}_2\text{Ge}$ and $P6_222\text{-SiGe}_2$ are 150 GPa and 134 GPa, respectively, showing that the E is decreased gradually with the increase of the Ge/Si ratio.

Meanwhile, it should be noted that the ν is basically associated with the B/G value, and the ductility will be exhibited with the ν being larger than 0.26, and the brittleness will display with the ν being less than 0.26 [48]. It can be seen clearly from Table II that the ν value of $P6_222\text{-Si}_2\text{Ge}$ (0.21) is slightly larger than that of SiGe_2 (0.19), and both of them are less than 0.26. Therefore, the proposed two $P6_222$ Si-Ge alloys are characterized as brittle. This conclusion is drawn consistently with the implication of B/G value mentioned above that $P6_222\text{-SiGe}_2$ displays the most brittle feature while diamond-Ge shows the least brittle feature.

The elastic anisotropy of crystal materials need to be put a great deal of emphasis to study, as its discrepancy along different directions can provide us with a concrete conclusion of the physical and chemical properties of crystal materials in different directions. For comparison, we study the anisotropy in terms of investigating the Young's modulus, shear modulus, and Poisson's ratio for Si_2Ge , SiGe_2 , Si_3 and Ge_3 in $P6_222$ phase, and detailed analysis about these issues is especially helpful to understand the mechanisms of crystal materials. It is known from other references [49–52] that, for isotropic materials, the 3D contour surface of the Young's modulus, shear modulus, and Poisson's ratio should exhibit a spherical shape. Otherwise, any deviation occurring from the spherical shape indicates the variations of physical, chemical and other natural aspects of materials along different axes, that is to say, the anisotropy appears.

The related results of the three-dimensional (3D) directional dependence of Young's modulus E for Si_2Ge , SiGe_2 , Si_3 and Ge_3 in $P6_222$ phase are shown in FIG. 3. It is seen that all the four crystal materials in $P6_222$ phase exhibit elastic anisotropy in terms of the Young's modulus, as all the 3D contour surfaces shown in FIG.

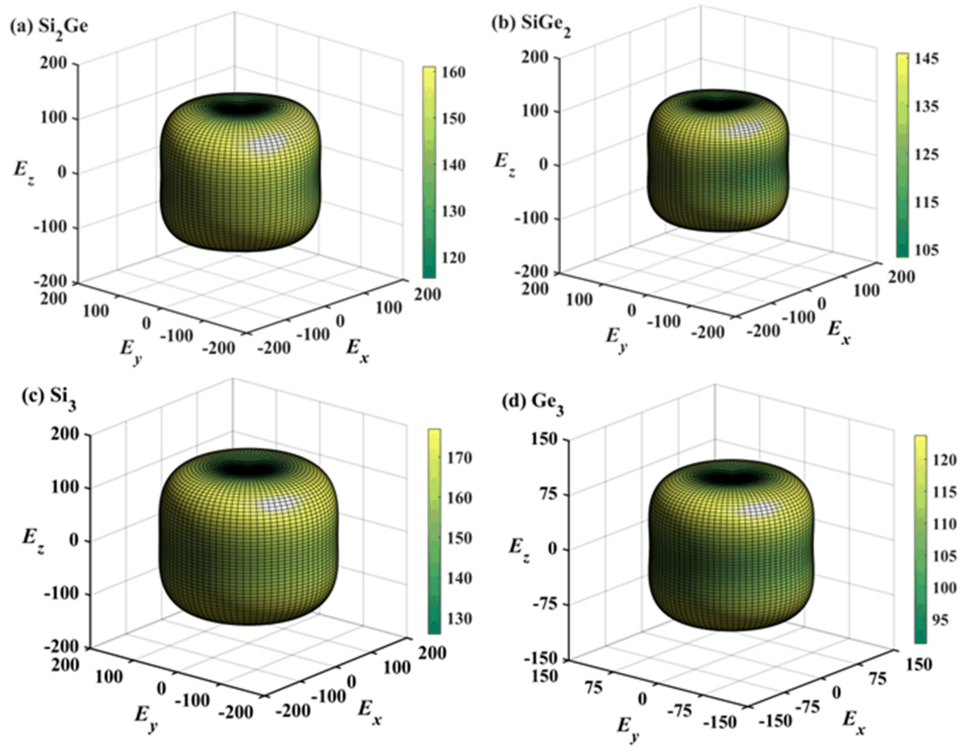


FIG. 3 The 3D surface construction of Young's modulus for (a) Si₂Ge, (b) SiGe₂, (c) Si₃ and (d) Ge₃ in *P*6₂22 phase.

3 appear in non-spherical shapes. In order to compare all the four crystal materials in detail related to the anisotropy, we use the ratios of the maximum to minimum value (E_{\max}/E_{\min}) to measure the elastic anisotropy in different planes, including the (100) plane, (010) plane, (001) plane, (011) plane, (101) plane, (110) plane and (111) plane, as listed in Table III. The E_{\max}/E_{\min} of Si₂Ge and SiGe₂ are almost the same in the (100), (010) and (110) planes, and have the identical values in the (001), (011) and (111) planes. Meanwhile, it is found that both of Si₂Ge and SiGe₂ show the greatest anisotropic property in the (010) plane with the largest E_{\max}/E_{\min} value of 1.39 (Si₂Ge: 160.88/115.50) and 1.41 (SiGe₂: 145.94/103.42), respectively, and show the weakest anisotropic property in the (001) plane with the same smallest E_{\max}/E_{\min} value of 1.07. It is seen that both of Si₃ and Ge₃ show the isotropic property in the (001) plane with the E_{\max}/E_{\min} value of 1.00. Also, it is interesting to find that both of Si₂Ge and SiGe₂ show approximate isotropic property in the (011) plane, as the E_{\max}/E_{\min} value is close to 1.00. Among all the four crystal materials, the E_{\max}/E_{\min} value of Si₃ in the (100), (010) and (110) planes has the largest value of 1.41, and the E_{\max}/E_{\min} value of SiGe₂ in the (010) plane also has the largest value of 1.41, indicating that both Si₃ and SiGe₂ exhibit the greater anisotropy than other materials in these mentioned planes.

The 3D surface constructions of shear modulus and Poisson's ratio for Si₂Ge, SiGe₂, Si₃ and Ge₃ in *P*6₂22

phase are shown in FIG. 4 and FIG. 5, respectively. As seen in FIG. 4 and FIG. 5, the maximum values of the shear modulus G_{\max} and Poisson's ratio ν_{\max} are represented by the red and orange surfaces, respectively, which are formed with the external dotted lines, and the minimum values G_{\min} and ν_{\min} are represented by the blue and purple surfaces, respectively, which are plotted with the internal solid lines. It can be seen from FIG. 4 and FIG. 5 that all the surface constructions of shear modulus and Poisson's ratio for Si₂Ge, SiGe₂, Si₃ and Ge₃ in *P*6₂22 phase exhibit distinctive non-spherical shapes, showing that the distribution of both shear modulus and Poisson's ratio appear elastic anisotropy with varying degrees.

Additionally, the distribution of G and ν in the (100), (010), (001), (011), (101), (110) and (111) planes, and the ratios of the maximum to minimum values (E_{\max}/E_{\min} and G_{\max}/G_{\min}) are also listed in Table III. Different from Young's modulus, both of G_{\max} for Si₂Ge (70.60 GPa) and SiGe₂ (65.47 GPa) exist in the same planes, such as the (100), (010), (001) and (110) planes, while both of G_{\min} values for Si₂Ge (48.91 GPa) and SiGe₂ (43.33 GPa) only exist in the (011) plane. It is also seen that both of Si₃ and Ge₃ show the same anisotropy with the G_{\max}/G_{\min} value of 1.41 and 1.45, respectively, in the (100), (010), (011), (101), (110) and (111) planes. Furthermore, it can be seen clearly that all the four crystal materials show the weakest anisotropy in the (001) plane, as the

TABLE III The maximum and minimum values of Young's modulus E_{\max} and E_{\min} (in GPa), shear modulus G_{\max} and G_{\min} (in GPa), and Poisson's ratio ν_{\max} and ν_{\min} for $P6_222\text{-Si}_{3-x}\text{Ge}_x$ ($x=0, 1, 2, 3$) in the primary planes.

Plane	E_{\max}				E_{\min}				E_{\max}/E_{\min}			
	Si ₃	Si ₂ Ge	SiGe ₂	Ge ₃	Si ₃	Si ₂ Ge	SiGe ₂	Ge ₃	Si ₃	Si ₂ Ge	SiGe ₂	Ge ₃
(100)	177.22	158.98	145.07	123.77	126.12	115.50	103.42	91.24	1.41	1.38	1.40	1.36
(010)	177.22	160.88	145.94	123.77	126.12	115.50	103.42	91.24	1.41	1.39	1.41	1.36
(001)	159.23	152.23	135.19	106.42	159.12	137.78	122.38	106.42	1.00	1.10	1.10	1.00
(011)	177.22	159.66	144.08	123.77	159.23	149.66	135.18	106.42	1.11	1.07	1.07	1.16
(101)	177.22	159.85	144.04	123.77	159.23	142.81	122.53	106.42	1.11	1.12	1.18	1.16
(110)	177.22	159.36	143.91	123.77	126.12	115.50	103.42	91.24	1.41	1.38	1.39	1.36
(111)	177.22	160.97	145.54	123.77	159.23	138.93	125.00	106.24	1.11	1.16	1.16	1.16
Plane	G_{\max}				G_{\min}				G_{\max}/G_{\min}			
	Si ₃	Si ₂ Ge	SiGe ₂	Ge ₃	Si ₃	Si ₂ Ge	SiGe ₂	Ge ₃	Si ₃	Si ₂ Ge	SiGe ₂	Ge ₃
(100)	77.52	70.60	65.47	55.06	54.83	49.53	43.34	38.09	1.41	1.42	1.51	1.45
(010)	77.52	70.60	65.47	55.06	54.83	50.61	45.58	38.09	1.41	1.39	1.44	1.45
(001)	77.52	70.60	65.47	55.06	69.54	64.43	55.93	47.39	1.11	1.09	1.17	1.16
(011)	77.52	67.84	62.10	55.06	54.83	48.91	43.33	38.09	1.41	1.39	1.43	1.45
(101)	77.52	68.49	65.45	55.06	54.83	49.73	44.79	38.09	1.41	1.38	1.46	1.45
(110)	77.52	70.60	65.47	55.06	54.83	48.94	43.91	38.09	1.41	1.44	1.49	1.45
(111)	77.52	70.57	64.01	55.06	54.83	49.42	43.34	38.09	1.41	1.43	1.48	1.45
Plane	ν_{\max}				ν_{\min}				ν_{\max}/ν_{\min}			
	Si ₃	Si ₂ Ge	SiGe ₂	Ge ₃	Si ₃	Si ₂ Ge	SiGe ₂	Ge ₃	Si ₃	Si ₂ Ge	SiGe ₂	Ge ₃
(100)	0.32	0.33	0.32	0.31	0.12	0.11	0.09	0.11	2.67	3.00	3.56	2.82
(010)	0.32	0.33	0.33	0.31	0.12	0.11	0.10	0.11	2.67	3.00	3.30	2.82
(001)	0.32	0.34	0.33	0.31	0.14	0.10	0.09	0.12	2.29	3.40	3.67	2.58
(011)	0.32	0.33	0.33	0.31	0.12	0.11	0.10	0.11	2.67	3.00	3.30	2.82
(101)	0.32	0.33	0.32	0.31	0.12	0.11	0.09	0.11	2.67	3.00	3.56	2.82
(110)	0.32	0.32	0.32	0.31	0.12	0.11	0.11	0.11	2.67	3.00	2.91	2.82
(111)	0.32	0.32	0.32	0.31	0.12	0.11	0.10	0.11	2.67	3.00	3.20	2.82

G_{\max}/G_{\min} values are the smallest one in all the different planes. At the same time, it is obvious that the elastic anisotropy of Si₂Ge is weaker than that of SiGe₂ in the shear modulus and Poisson's ratio, as the G_{\max}/G_{\min} and ν_{\max}/ν_{\min} values of SiGe₂ are always larger than those of Si₂Ge along each different plane. The ν_{\max} and ν_{\min} of Si₂Ge are 0.34 and 0.10, respectively, and the maximum value of ν_{\max}/ν_{\min} is 3.40 in the (001) plane. The ν_{\max} and ν_{\min} of SiGe₂ are 0.33 and 0.09, respectively, and the maximum value of ν_{\max}/ν_{\min} is 3.67 in the (001) plane, which is obviously larger than that of Si₂Ge. Again, this firmly proves that the anisotropy of these proposed Si-Ge alloys in $P6_222$ phase is $\text{Si}_2\text{Ge} < \text{SiGe}_2$.

The Debye temperatures Θ_D of Si₃, Si₂Ge, SiGe₂ and Ge₃ in $P6_222$ phase, as well as Si and Ge in diamond phase, are calculated using the semi-empirical formula

$$\Theta_D = v_m \frac{h}{k_B} \left(\frac{3n N_A \rho}{4\pi M} \right)^{1/3} \quad (1)$$

where v_m is expressed as $\left[\frac{(2/v_s^3 + 1/v_p^3)}{3} \right]^{-1/3}$ [53],

$v_s = \left(\frac{G}{\rho} \right)^{1/2}$, $v_p = \left[\frac{(B + 4G/3)}{\rho} \right]^{1/2}$ [54], h is the Planck's constant, k_B the Boltzmann's constant, n is the number of atoms in the molecule, N_A the Avogadro's number, ρ is the density, and M is the molecular weight. Herein, v_m represents the mean sound velocity; v_s and v_p represent the transverse and longitudinal sound velocities, respectively. The calculated Debye temperature and sound velocities of the four crystal materials in $P6_222$ phase, as well as Si and Ge in diamond phase are listed in Table IV. It is seen that the values of Θ_D in diamond phase are 639 K (Si) and 360 K (Ge), which are in excellent agreement with the previously reported work of 652 K (Si) and 374 K (Ge) in Ref.[55]. Due to the densities of Si₃, Si₂Ge, SiGe₂ and Ge₃ in $P6_222$ phase gradually get higher (see Table I), and the bulk modulus B and shear modulus G of these four crystal materials correspondingly decreases (see Table II), the order of Θ_D for these four crystal materials is $P6_222\text{-Si}_3$ (625 K) $>$ $P6_222\text{-Si}_2\text{Ge}$ (501 K) $>$ $P6_222\text{-SiGe}_2$ (414 K) $>$ $P6_222\text{-Ge}_3$ (345 K). This also results in the sound velocities (v_p , v_s and v_m) of Si₃, Si₂Ge, SiGe₂ and Ge₃ in $P6_222$ phase reduc-

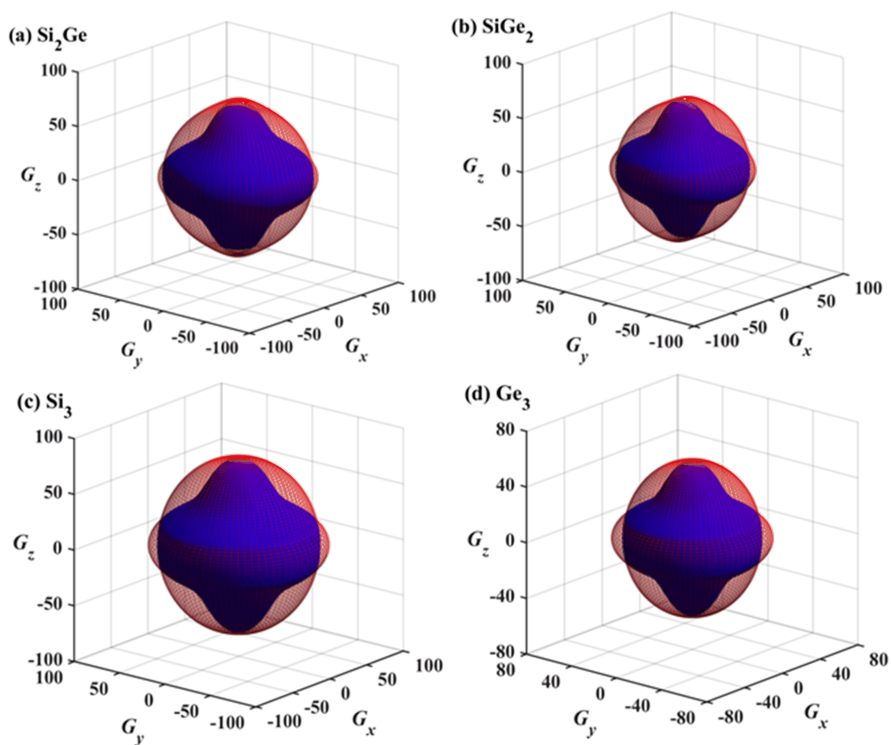


FIG. 4 The 3D contour surfaces of shear modulus for (a) Si₂Ge, (b) SiGe₂, (c) Si₃ and (d) Ge₃ in $P6_222$ phase.

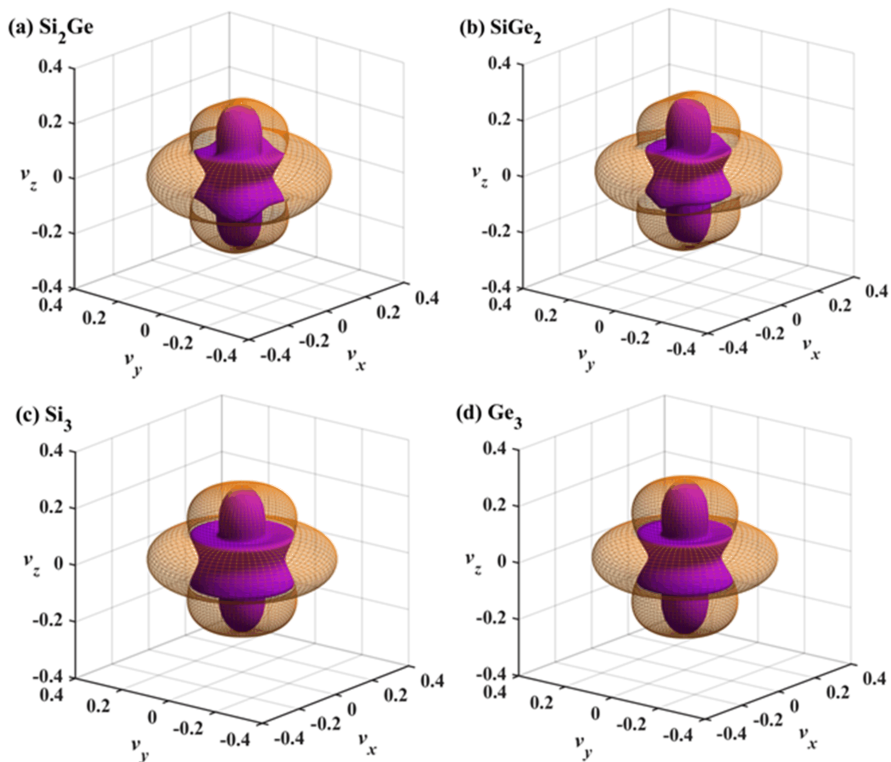


FIG. 5 The 3D directional dependence of Poisson's ratio for (a) Si₂Ge, (b) SiGe₂, (c) Si₃ and (d) Ge₃ in $P6_222$ phase.

TABLE IV The Debye temperature (Θ_D in K), and the longitudinal, transverse, mean sound velocity (v_p , v_s , v_m in m/s) of $\text{Si}_{3-x}\text{Ge}_x$ ($x=0, 1, 2, 3$) in $P6_222$ phase.

Materials	Θ_D	v_p	v_s	v_m
$P6_222\text{-Si}_3$	625	8470	5140	5679
$P6_222\text{-Si}_2\text{Ge}$	501	6694	4071	4498
$P6_222\text{-SiGe}_2$	414	5570	3430	3785
$P6_222\text{-Ge}_3$	345	4761	2916	3219
Diamond-Si	639	8727	5303	5859
Diamond-Ge	360	5220	3119	3452
	652 [55]			
	374 [55]			

ing gradually with the increase of the incorporation of germanium atoms.

It is known that sound waves travel at different speeds along different directions in crystal materials, so anisotropy of sound velocities also needs to be discussed. The directions related to sound traveling in crystal materials are basically classified into two categories, the propagation direction and the polarizing direction. In hexagonal symmetry, sound velocities along the [001] and [100] propagation directions can be calculated by the following equations, respectively [56]:

For [010] plane:

$$[001]v_p = \sqrt{\frac{C_{33}}{\rho}}$$

$$[100]v_{s1} = [010]v_{s2} = \sqrt{\frac{C_{44}}{\rho}}$$

For [100] plane:

$$[100]v_p = \sqrt{\frac{C_{11} - C_{12}}{2\rho}}$$

$$[010]v_{s1} = \sqrt{\frac{C_{11}}{\rho}}$$

$$[001]v_{s2} = \sqrt{\frac{C_{44}}{\rho}}$$

where v_p is the longitudinal sound velocity, and v_{s1} and v_{s2} are the transverse sound velocities in the first and second mode, respectively.

The anisotropic sound velocities of Si_2Ge and SiGe_2 in $P6_222$ phase are listed in Table V. It can be seen that the highest sound velocities of $P6_222\text{-Si}_2\text{Ge}$ and $P6_222\text{-SiGe}_2$ are the transverse sound velocity in the [100] propagation direction, which are 8478 m/s and 4667 m/s, respectively, both appear in the second mode. Also, it is found that the sound velocities of $P6_222\text{-Si}_2\text{Ge}$ along different directions are all largely higher than those of $P6_222\text{-SiGe}_2$. This is

TABLE V The calculated anisotropic sound velocities of Si_2Ge and SiGe_2 in $P6_222$ phase.

Propagation direction	Polarization direction	Velocity/(m/s)	
		$P6_222\text{-Si}_2\text{Ge}$	$P6_222\text{-SiGe}_2$
[001]	[001] v_p	7785	4473
	[100] v_{s1}	5505	3121
	[010] v_{s2}	5505	3121
[100]	[100] v_p	5214	2900
	[010] v_{s1}	8478	4667
	[001] v_{s2}	5505	3121

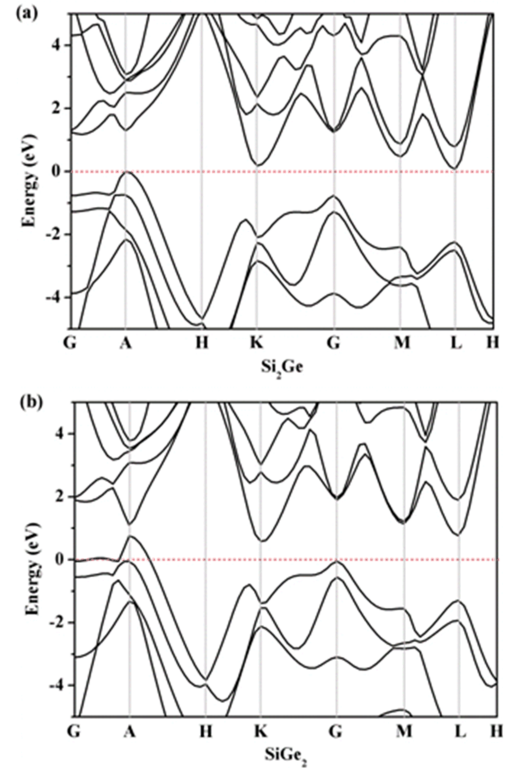


FIG. 6 The electronic band structures of (a) Si_2Ge and (b) SiGe_2 in $P6_222$ phase.

due to the fact that the dominant elastic constants of $P6_222\text{-Si}_2\text{Ge}$, including C_{11} , C_{33} and C_{44} , largely outweigh those of $P6_222\text{-SiGe}_2$, even though the density of $P6_222\text{-Si}_2\text{Ge}$ (3.742 g/cm^3) is smaller than that of $P6_222\text{-SiGe}_2$ (4.760 g/cm^3). Meanwhile, it is obvious that in the [001] propagation direction, both of $P6_222\text{-Si}_2\text{Ge}$ and $P6_222\text{-SiGe}_2$ exhibit the identical transverse sound velocity in the first and second mode.

The electronic band structures of Si_2Ge and SiGe_2 in $P6_222$ phase calculated by the HSE06 function are shown in FIG. 6. It is seen that the Fermi level (0 eV) is represented by the dashed line, and the maximum-energy state in the valence band and the minimum-energy state in the conduction band are each labeled by a certain crystal momentum (k -vector) across the Brill-

loun zone. The coordinates of high symmetry points across the Brillouin zone for Si₂Ge and SiGe₂ in *P*6₂22 phase are G (0.000, 0.000, 0.000)→A (0.000, 0.000, 0.500)→H (-0.333, 0.667, 0.500)→K (-0.333, 0.667, 0.000)→G (0.000, 0.000, 0.000)→M (0.000, 0.500, 0.000)→L (0.000, 0.500, 0.500)→H (-0.333, 0.667, 0.500). As can be seen, the valence band maximums (VBM) of *P*6₂22-Si₂Ge is located at the A point, and the conduction band minimums (CBM) is located at the L point. Obviously, *P*6₂22-Si₂Ge is an indirect band gap semiconductor and the band gap is 0.07 eV. The CBM of *P*6₂22-SiGe₂ is located at the K point, while its valence bands along G-H direction exhibit the metallic feature as the top dispersive band crossing into the upper region above the Fermi level with positive energies.

IV. CONCLUSION

The physical properties of two novel group 14 element alloys Si₂Ge and SiGe₂ in *P*6₂22 phase were investigated by using first-principles computations in this work, which include the structural properties, stability, elastic anisotropy properties, electronic properties and thermodynamic properties. The crystal structures of Si_{3-x}Ge_x (*x*=0, 1, 2, 3) in *P*6₂22 phase are all in hexagonal symmetry, and their densities get higher gradually with increasing the incorporation of germanium atoms. By illustrating the 3D surface constructions of Young's modulus, shear modulus and Poisson's ratio for the Si₂Ge and SiGe₂ in *P*6₂22 phase, as well as discussing and comparing the differences with *P*6₂22-Si₃ and *P*6₂22-Ge₃, we found that the elastic anisotropy of *P*6₂22-Si₂Ge is weaker than that of *P*6₂22-SiGe₂. Additionally, the electronic band structures were calculated by HSE06 hybrid functional, indicating that *P*6₂22-Si₂Ge is an indirect band gap semiconductor, and *P*6₂22-SiGe₂ exhibits the metallic feature. Finally, the Debye temperature and sound velocities were analyzed to study the thermodynamic properties of the proposed *P*6₂22-Si₂Ge and *P*6₂22-SiGe₂.

V. ACKNOWLEDGMENTS

This work was supported by the National Natural Science Foundation of China (No.61804120), the Scientific Research Program of Shaanxi Provincial Education Department (19JK0471), and the Science and Technology Foundation for Youths of Xi'an University of Architecture and Technology (QN1625).

- [1] Q. Y. Fan, J. Xu, W. Z. Zhang, Y. X. Song, and S. N. Yun, *J. Appl. Phys.* **126**, 045709 (2019).

- [2] Q. Y. Fan, W. Z. Zhang, Y. X. Song, W. Zhang, and S. N. Yun, *Semicond. Sci. Technol.* **35**, 055012 (2020).
- [3] Q. Y. Fan, H. Q. Wang, W. Z. Zhang, M. F. Wei, Y. X. Song, W. Zhang, and S. N. Yun, *Current Appl. Phys.* **19**, 1325 (2019).
- [4] R. L. Zhou, B. Y. Qu, B. Zhang, P. F. Li, and X. C. Zeng, *J. Mater. Chem. C* **2**, 6536 (2014).
- [5] C. Y. He, C. X. Zhang, J. Li, X. Y. Peng, L. J. Meng, C. Tang, and J. X. Zhong, *Phys. Chem. Chem. Phys.* **18**, 9682 (2016).
- [6] Q. Y. Fan, C. C. Chai, Q. Wei, and Y. T. Yang, *Phys. Chem. Chem. Phys.* **18**, 12905 (2016).
- [7] D. Y. Kim, S. Stefanoski, O. O. Kurakevych, and T. A. Strobel, *Nat. Mater.* **14**, 169 (2015).
- [8] S. Q. Wang and H. Q. Ye, *J. Phys. Condens. Matter* **15**, 5307 (2003).
- [9] Q. Y. Fan, C. C. Chai, Q. Wei, Y. T. Yang, Q. Yang, P. Y. Chen, M. H. Xing, J. Q. Zhang, and R. H. Yao, *J. Solid State Chem.* **233**, 471 (2016).
- [10] I. H. Lee, J. Y. Lee, Y. J. Oh, S. Kim, and K. J. Chang, *Phys. Rev. B* **90**, 115209 (2014).
- [11] Q. Q. Wang, B. Xu, J. Sun, H. Y. Liu, Z. S. Zhao, D. L. Yu, C. Z. Fan, and J. L. He, *J. Am. Chem. Soc.* **136**, 9826 (2014).
- [12] Q. Y. Fan, Y. B. Zhao, X. H. Yu, Y. X. Song, W. Zhang, and S. N. Yun, *Diamond Rel. Materials* **106**, 107831 (2020).
- [13] Y. J. Oh, In-Ho Lee, S. Kim, J. Lee, and K. J. Chang, *Sci. Rep.* **5**, 18086 (2015).
- [14] A. Mujica, C. J. Pickard, and R. J. Needs, *Phys. Rev. B* **91**, 214104 (2015).
- [15] M. Amsler, S. Botti, M. A. L. Marques, and T. J. Lenosky, S. Goedecker, *Phys. Rev. B* **92**, 014101 (2015).
- [16] S. Botti, J. Flores-Livas, M. Amsler, S. Goedecker, and M. Marques, *Phys. Rev. B* **86**, 121204 (2012).
- [17] Q. Y. Fan, H. Q. Wang, Y. X. Song, W. Zhang, and S. N. Yun, *Comput. Mater. Sci.* **178**, 109634 (2020).
- [18] Q. Y. Fan, C. C. Chai, Q. Wei, Q. Yang, and Y. T. Yang, *Mater. Sci. Semicond. Process.* **43**, 187 (2016).
- [19] Y. H. Zhang, C. C. Chai, Q. Y. Fan, Y. T. Yang, and M. J. Xing, *Chin. J. Phys.* **54**, 298 (2016).
- [20] Q. Y. Fan, C. C. Chai, Q. Wei, K. Q. Wong, Y. Q. Liu, and Y. T. Yang, *J. Mater. Sci.* **53**, 2785 (2018).
- [21] Q. Y. Fan, C. C. Chai, Q. Wei, P. Zhou, and Y. Yang, *Mater. Design* **132**, 539 (2017).
- [22] K. Moriguchi, S. Munetoh, and A. Shintani, *Phys. Rev. B* **62** (2000) 7138.
- [23] F. Schäffler, *Semicond. Sci. Technol.* **12**, 1515 (1997).
- [24] Q. Y. Fan, R. Niu, W. Z. Zhang, W. Zhang, Y. C. Ding, and S. N. Yun, *ChemPhysChem* **20**, 128 (2019).
- [25] Y. X. Song, C. C. Chai, Q. Y. Fan, W. Zhang, Y. T. Yang, *J. Phys.: Condens. Matter* **31**, 255703 (2019).
- [26] Q. Y. Fan, R. L. Yang, W. Zhang, S. N. Yun, *Results Phys.* **15**, 102580 (2019).
- [27] Q. Y. Fan, C. C. Chai, Q. Wei, H. Y. Yan, Y. B. Zhao, Y. T. Yang, X. H. Yu, Y. Liu, M. J. Xing, J. Q. Zhang, and R. H. Yao, *J. Appl. Phys.* **118**, 185704 (2015).
- [28] Y. G. Guo, Q. Wang, Y. Kawazoe, and P. A. Jena, *Sci. Rep.* **5**, 14342 (2015).
- [29] Q. Y. Fan, C. C. Chai, Q. Wei, P. K. Zhou, J. Q. Zhang, and Y. T. Yang, *Materials* **9**, 284 (2016).
- [30] W. Zhang, C. C. Chai, Q. Y. Fan, Y. X. Song, and Y. T. Yang, *ChemNanoMat* **6**, 139 (2020).

- [31] Z. S. Zhao, F. Tian, X. Dong, Q. Li, Q. Q. Wang, H. Wang, X. Zhong, B. Xu, D. L. Yu, J. L. He, H. T. Wang, Y. M. Ma, and Y. J. Tian, *J. Am. Chem. Soc.* **134**, 12362 (2012).
- [32] P. Hohenberg and W. Kohn, *Phys. Rev.* **136**, B864 (1964).
- [33] W. Kohn and L. J. Sham, *Phys. Rev.* **140**, A1133 (1965).
- [34] S. J. Clark, M. D. Segall, C. J. Pickard, P. J. Hasnip, M. Probert, K. Refson, and M. C. Payne, *Z. Kristallogr* **220**, 567 (2005).
- [35] J. P. Perdew, K. Burke, and M. Ernzerhof, *Phys. Rev. Lett.* **77**, 3865 (1996).
- [36] B. G. Pfrommer, M. Cote, S. G. Louie, and M. L. Cohen, *J. Comput. Phys.* **131**, 233 (1997).
- [37] S. Baroni, S. De Gironcoli, A. Dal Corso, and P. Gianozzi, *Rev. Mod. Phys.* **73**, 515 (2001).
- [38] J. Heyd, G. E. Scuseria, and M. J. Ernzerhof, *J. Chem. Phys.* **118**, 8207 (2003).
- [39] H. J. Monkhorst and J. D. Pack, *Phys. Rev. B* **13**, 5188 (1976).
- [40] Y. B. Zhao, W. Zhang, and Q. Y. Fan, *Commun. Theor. Phys.* **71**, 1036 (2019).
- [41] D. R. Lide, *Handbook of Chemistry and Physics, (73rd Edn.)*, Florida: Chemical Rubber (1994)
- [42] Z. Z. Li, J. T. Wang, L. F. Xu, and C. F. Chen, *Phys. Rev. B* **94**, 174102 (2016).
- [43] M. Grimsditch, E. S. Zouboulis, and A. Polian, *J. Appl. Phys.* **76**, 832 (1994).
- [44] R. Gomez-Abal, X. Li, M. Scheffler, and C. Ambrosch-Draxl, *Phys. Rev. Lett.* **101**, 106404 (2008).
- [45] B. B. Karki, G. J. Ackland, and J. Crain, *J. Phys.: Condens. Matter* **9**, 8579 (1997).
- [46] X. Z. Li and M. J. Xing, *Comput. Mater. Sci.* **158**, 170 (2019).
- [47] S. F. Pugh, *Philos Mag.* **45**, 823 (1954).
- [48] M. J. Xing, B. H. Li, Z. T. Yu, and Q. Chen, *J. Mater. Sci.* **50**, 7104 (2015).
- [49] Q. Y. Fan, Z. Duan, Y. X. Song, W. Zhang, Q. D. Zhang, and S. N. Yun, *Electron. Mater.* **12**, 3589 (2019).
- [50] Q. D. Zhang, Y. C. Zou, Q. Y. Fan, and Y. T. Yang, *Materials* **13**, 1280 (2020).
- [51] W. Zhang, C. C. Chai, Q. Y. Fan, Y. X. Song, and Y. T. Yang, *J. Appl. Phys.* **126**, 145704 (2019).
- [52] Q. Y. Fan and W. Z. Zhang, S. N. Yun, J. Xu, and Y. X. Song, *Chem. Eur. J.* **24**, 17280 (2018).
- [53] O. L. Anderson, *J. Phys. Chem. Solids* **24**, 909 (1963).
- [54] K. B. Panda and K. S. Ravi, *Comput. Mater. Sci.* **35**, 134 (2006).
- [55] H. Siethoff and K. Ahiborn, *Phys. Status Solidi B* **190**, 179 (1995).
- [56] Y. H. Duan, Y. Sun, M. J. Peng, and S. G. Zhou, *J. Alloys Compd.* **595**, 14 (2014).